Tellus (1999), 51A, 880–901
Printed in UK. All rights reserved

TELLUS
ISSN 0280–6495

The sensitivity of supercritical atmospheric boundary-layer flow along a coastal mountain barrier

By MICHAEL TJERNSTRÖM, *Department of Meteorology, Stockholm University, Stockholm, Sweden*

(Manuscript received 30 September 1998; in final form 18 June 1999)

ABSTRACT

Hypothetical numerical simulations are carried out to investigate the sensitivity of a coastally-trapped supercritical flow to various forcing. All simulations are compared with a control simulation, that is based on a real case from the coastal waves field experiment off the coast of California in 1996, the 7 June case. This case features a northerly supercritical flow along the California coast that triggers an expansion fan at Cape Mendocino (40.4°N, 124.4°W). The upstream jet then strengthens as the boundary layer becomes more shallow. Other important features are the terrain at the cape and the SST depression into Shelter Cove in the lee of the cape. All sensitivity simulations reveal an expansion fan with the associated dynamics; this appears to be a very stable feature. Altering the local terrain changes the local structure of the jet and removes the lee-wave that is responsible for the apparent collapse of the boundary layer in Shelter Cove. A realistic SST, instead of a spatially constant value, has only minor effects very locally. Changing the Froude number of the flow by manipulation of the inversion strength reveals an unexpected feedback. A weaker inversion increases the entrainment and thus deepens the boundary layer, and vice versa, while increasing the inversion strength. In the expression for the Froude number, these 2 effects cancel and the end results is very similar to the control run. Even when reducing the background flow speed by 50%, an expansion fan appeared. This case is thus transcritical–subcritical upstream, turning supercritical at the cape. It experiences the largest changes in terms of wind speed. Attempts to generate a solid stratocumulus layer (no clouds were present in reality) in the model failed. Within a realistic increase of the initial boundary layer humidity, it was not possible to maintain clouds in these runs. In summary, the expansion fan dynamics appear strong and quite consistent, and it was virtually impossible to find a set of conditions, based on perturbations to the control case, that did not reveal supercriticality and the expansion fan dynamics.

1. Introduction

Within shallow-water theory for a rotating system, inertio-gravity waves at the interface between two homogeneous fluids with different density, redistribute mass within the lower fluid towards geostrophic balance. The fastest of these waves, the shallow-water gravity wave, travel at a phase speed of $c=(g'H)^{1/2}$. Here, H is the depth of the lower fluid, $g'=(\Delta\rho/\rho_0)g$ is the reduced gravity while $\Delta\rho$ is the density difference over the interface between the two fluids and ρ_0 is the density of the lower fluid. For this reason, the theory is sometimes also referred to as "single-layer reduced-gravity flow", thus ignoring the upper fluid. If the velocity of the lower fluid, U, is higher than the phase speed, the Froude number ($\mathrm{Fr}=U(g'H)^{-1/2}$) is lager than unity, and the flow is referred to as supercritical. This (shallow-water) definition of Fr will be used throughout this paper; however, the reduced gravity will for convenience be defined using the potential temperature, θ, rather than the density; $g'=(\Delta\theta/\theta_0)g$. Physically, supercriticality means that geostrophic adjustment

* E-mail: michaelt@misu.su.se.

can only take place downstream of a local perturbation in the pressure field, as no information on a local perturbation in mass (or pressure) can propagate upstream. If such a flow is bounded by a sidewall higher than the depth of the lower fluid, the flow becomes sensitive to changes in the orientation of that wall. If the wall turns "away" from the flow, i.e., the channel is widening, an expansion fan will form (Baines, 1995). In the fan, the depth of the lower fluid decreases and the flow accelerates. It will start at the point where the wall changes direction and widen, forming an angle to the flow, determined by the upstream Fr, as gravity waves propagate perpendicular to the flow while being advected downstream. If the wall turns back "into" the flow again, the flow will experience a blocking. If this blocking brings the velocity down so that $U < c$, the flow becomes subcritical locally and a hydraulic jump will occur along the line where $\mathrm{Fr} = 1$ ($U = c$), as all the gravity-waves downstream of this line propagating against the flow will converge here.

In the atmosphere, this type of flow may appear in a marine atmospheric boundary layer (MABL) capped by a strong inversion, along a mountainous coastline with coastal mountains higher than the MABL depth (Winant et al., 1988). These conditions are thus often observed along the west coast of the United States. For much of this coast, the height of the coastal mountains exceeds 400 m, forming an almost continuous barrier from Oregon to southern California. The strength of the inversion capping the MABL is typically $\Delta\theta =$ 10–20 K in summer (Dorman and Winant, 1995) and these conditions can be persistent for long periods, maintained from above by subsidence and from below by turbulent mixing in the MABL. The density of the cooler MABL air is thus typically $\sim 5\%$ higher than the air above the inversion, and Winant et al. (1988) showed that the flow can be treated as a single-layer reduced-gravity flow. Winant et al. (1988) provide the first detailed in situ observations of such an event, during the CODE experiment (Beardsley et al., 1987). In airborne measurements between Point Arena and Bodega Bay along the northern California coast, they observed both a strong acceleration, later interpreted as an expansion fan, and an abrupt transition in a hydraulic jump. This case was analyzed, using non-rotating single-layer reduced-gravity flow theory.

Several factors contribute to making the atmosphere more complex than the shallow-water theory allows. Along the US west coast, the strong northerly flow is controlled partly by large scale dynamics, causing the inversion — the fluid interface — to slope gently from around ~ 2000 m near Hawaii to O(100 m) near the US west coast. This represents the effect of the subsidence from the North Pacific summertime subtropical high (Neiburger et al., 1961). Within a Rossby radius of deformation O(10–100 km) from the coast, the slope becomes stronger, due to the interplay with a diurnal thermally driven cross-coast flow (Beardsley et al., 1987). The sloping inversion introduces a mesoscale thermal wind (Zemba and Friche, 1987), with increasing strength approaching the coast. Although the typical northwesterly background wind, between the North Pacific high and the thermal low over southwestern US, is only 5–10 ms^{-1}, the local wind speed in the coastal low-level jet often exceeds 20 ms^{-1} (Beardsley et al., 1987; Dorman and Winant, 1995; Burk and Thompson, 1996; Cui et al., 1998; Rogers et al., 1998). Since the terrain barrier impedes geostrophic adjustment, Overland (1984) argued that the flow under such conditions is semi-geostrophic, geostrophic in the cross-shore component, while in the along-shore component the pressure gradient must be balanced by either ageostrophic acceleration, as for "gap winds", or by surface friction; turbulence thus also plays an important rôle. Samelson and Lentz (1994) confirmed these ideas in an analysis of buoy observations in a limited region around Point Arena (Fig. 1). Another consequence of the surface friction is coastal upwelling, caused by a net Ekman transport of surface water off-shore, which promotes upwelling of cool water to the surface. The observed depression of the sea surface temperature (SST) in the near-coast zone is often several degrees, providing a heterogeneous surface forcing. Stratocumulus clouds or fog often form below the inversion, and this also alters the MABL structure. The coastal MABL off the US west coast is often far from the horizontally homogeneous single-layer fluid assumed in simpler theory. Samson (1992) included rotation and surface friction in a non-linear single-layer reduced-gravity model and found that this improved the agreement with the observation. It explained the observed wind speed maximum at the coast, with the layer-depth

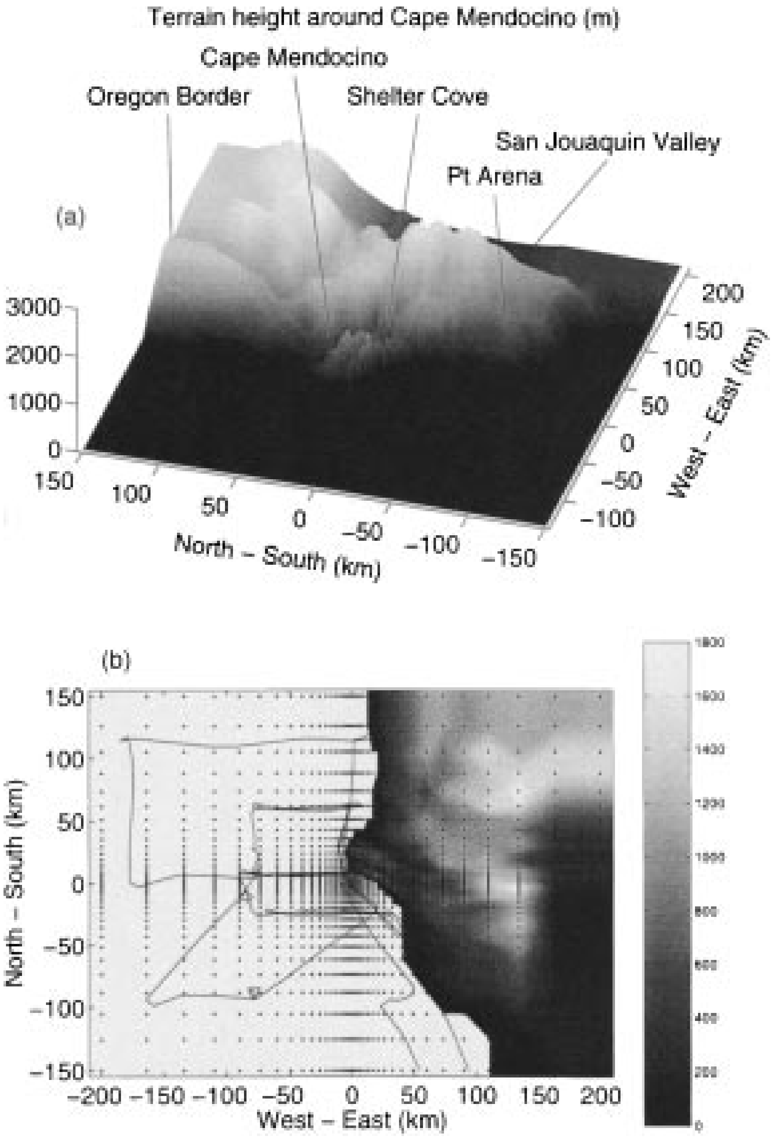

Fig. 1. Plots of (a) the model terrain surface indicating some locations and (b) contours of the model terrain also including the location of model grid points and the C-130 flight track for the research mission on 7 June 1996.

minimum somewhat downwind. As a consequence, the expansion fan critical lines, wind speeds, pressure and layer depths form a lens-shaped pattern, rather than straight lines radiating outward in a fan-shaped pattern from topographic bends, as predicted by simpler irrotational, frictionless hydraulic models.

These flows have a profound influence on the local wind climate along mountainous coasts, and the local wind speeds are often twice, or more, than those predicted with synoptic-scale models. A better understanding requires both more observations and detailed model studies. Even with the theoretical improvements discussed above, only the limited area around Point Arena had been adequately sampled, by aircraft measurements, to provide experimental evidence. It has thus been uncertain how representative these conditions are for the west coast of the US, or any other similar coast, although an analysis by Dorman and Winant (1995) indicated that these conditions could be quite frequent during summer at the US west coast. To study this in more detail, instrumented flights with a long-range research aircraft were performed out of Monterey, along the US west coast during the summer of 1996, the Coastal Waves 1996 program (Rogers et al., 1998). Several different research flights span the US west coast from Point Conception in the south to Cape Blanco in the north. During these missions, supercritical events were frequently encountered. Several of the cases from the experiment have subsequently been simulated with state-of-the-art mesoscale models; this has shed light on several important factors. This paper builds the simulation of the case from 7 June, at Cape Mendocino (40.4°N, 124.4°W), that was presented in Tjernström and Grisogono (1999, hereafter TG). This simulation indicated several important features: the apparent one-way interaction with the local ocean surface; the impact of local terrain features on the jet structure, and the importance of different terms in the momentum budget. In the present paper, several simulations based on this case are presented, performed for simplified background conditions while altering different aspects of the forcing. The aim is to investigate the sensitivity of the observed flow to (i) external forcing, (ii) internal structure and (iii) the presence of MABL clouds.

2. The field experiment

The Coastal Waves 1996 program is described in detail in Rogers et al. (1998). Extensive details from aircraft measurements around Point Sur are also presented in Dorman et al. (1999a). Conditions at Cape Mendocino are also described in Dorman and Rogers (1998), while Dorman et al. (1999b) provide a climatology from the experiment. Furthermore, see Burk and Haack (1998) for a study of special conditions around Pt Sur. The program consisted of a longer effort from May to September 1996, to obtain reliable average conditions and to capture the rare events of so called "southerly surges" (Bond et al., 1996), and a concentrated effort during the month of June. Automated surface weather stations, drifting and fixed buoys (including the NDBC buoy system), wind profilers, acoustic sounders and radiosoundings were available along the coast from southern California to the Oregon coast during the longer effort.

During the intensive operations period, a primary measurement platform was the National Center for Atmospheric Research (NCAR)* C-130 Hercules research aircraft. From 2 June to 1 July, the C-130 flew a total of 11 missions: 4 around Point Sur, 3 around Cape Mendocino, 3 around Point Conception and 1 around Cape Blanco. The standard suite of data from this platform include winds, temperature and humidity. Cloud liquid water, droplet and aerosol spectra were also collected as were atmospheric radiation and radiometric surface temperature. Most data are available at a low rate (1 Hz), while wind speed, temperature and humidity are also sampled at a higher rate (25 Hz), for calculation of turbulence moments by eddy-correlation technique. In addition, in this experiment, remote sensing of the MABL structure was provided by the Scanning Aerosol Backscatter Lidar (SABL), developed by the Atmospheric Technology Division (ATD) of NCAR. Flight level data from this platform form the backbone for the simulations presented in this paper.

3. The numerical experiment

3.1. The model

The numerical model is utilized as a numerical laboratory rather than as a forecast tool. The aim is to study the effect on the flow by several factors and the results here rest on the fact that the original model simulation agrees well with the observations. The effect of changes in the background or initial conditions, or in the surface forcing can then be studied by comparison of model results with a control simulation; such an experiment would be virtually impossible from the field experiment data only. Some of the modeling techniques applied here are motivated by this aim

* NCAR is supported by the National Science Foundation.

(Tjernström and Grisogono, 1996; Grisogono and Tjernström, 1996; Grisogono et al., 1998; Cui et al., 1998; TG). The leading idea is to attempt to simulate as much as possible of the observed flow with as simple forcing and background flow conditions as possible, while retaining a high degree of control of the forcing. This facilitates the interpretation of the sensitivity simulations and provides control over the numerical experiment.

The MIUU meso-γ-scale model, used here and in TG, is a 3D hydrostatic model with a higher-order turbulence closure. The turbulence closure is an improved, consistent version of the "level 2.5"-closure (Mellor and Yamada, 1982). It carries an improved description for the pressure re-distribution terms (the "near-wall" correction) and an algorithm to keep all 2nd-order moments realizable (Andrén, 1990). The model also includes routines for sub-grid scale condensation and radiation, as well as a surface energy balance, but the latter is not used here for the sake of simplicity. Detailed descriptions are found in Tjernström (1987a, b). Shorter descriptions are found in Tjernström (1988a) and Enger (1990a).

The model has previously been applied in a variety of applications including terrain-induced flows (Tjernström, 1987a; Enger, 1990a; Enger et al., 1993; Koracin and Enger, 1994; Grisogono, 1995; Enger and Grisogono, 1998), coastal flows (Cui et al., 1998; TG), dispersion calculations (Enger, 1990b), marine stratocumulus (Tjernström, 1988b; Tjernström and Koracin, 1995) and air chemistry (Svensson, 1998; Svensson and Klemm, 1998). It has thus been thoroughly examined for a variety of flows and is well documented.

The vertical coordinate is transformed into a terrain-influenced coordinate system according to Pielke (1984). The terrain was extracted from a ~ 500 m resolution terrain data-base available at NCAR, and averaged to the model grid. The horizontal grid expands towards the lateral boundaries, to achieve maximum resolution in the central parts of the domain, while locating the lateral boundaries far from the area of interest. A simple radiative boundary condition is applied at the lateral boundaries while a sponge layer is introduced at the model top (Grisogono, 1995). The vertical grid also expands, log-linearly, towards the model top. The maximum resolution is located close to the surface at the domain center ~ 20 km south of the tip of Cape Mendocino. The domain is $450 \times 350 \times 5$ km^3 and is resolved by $41 \times 41 \times 30$ grid points, with a maximum resolution 2×2 km^2 in the horizontal and 1 m vertically close to the surface. Fig. 1a shows the model terrain, along with some geographical references, while Fig. 1b shows the distribution of the model grid points and the flight track from the experiment on 7 June. The simulations were initialized using a dynamic initialization; the model is given horizontally homogeneous temperature, humidity and wind fields and run through a pre-integration period, during which the model fields adjust gradually to a realistic quasi-balance. The simulations presented here were all initialized at 1800 local standard time (LST) the day before the events, and no data for the first 12 h are used. Most results presented here are from 15.00 LST, 21 h into the simulation.

3.2. *The control simulation*

The SST was set constant in time and space at 12.5°C (except for in one sensitivity simulation, see below), while the diurnal temperature variation of the soil surface was prescribed using a sinusoidal-type function, as in TG. Similarly, specific humidity was specified at the surface using potential evaporation over the sea, and a fraction of this value over land. These conditions were transferred to the lower model boundary using matching surface-layer and roughness sub-layer similarity theories. Together, this allows the coastal land surfaces to be influenced by local advection of moist and cold air from the sea, and vive versa, while allowing for a strong experimental control over the surface forcing.

The background (synoptic scale) pressure gradient was specified as a geostrophic wind, for simplicity. The respective components of the geostrophic wind (u_g, v_g) changes linearly from $(-2, -15)$ ms^{-1} at the surface to (3.5, 4) ms^{-1} at 2500 m and to (9, 7.5) ms^{-1} at the model top, but are constant both in time and horizontally. These values were taken as in TG, i.e., extracted from weather charts with the aid of analysis of flight-level data. Thus the along-coast background flow reverses with height. However, the flow aloft is sufficiently weak to prohibit trapping of any vertically propagating gravity-waves; these will propagate to the model top and be absorbed by the sponge layer. Initial potential temperature and specific humidity profiles were taken as well-mixed (constant values) in an initially 800 m deep MABL, capped by a 17°C and 4 g kg^{-1} inversion with stable stratification and constant (1 g kg^{-1}) humidity aloft; all these values were also taken from the TG study.

3.3. *The sensitivity simulations*

Three sets of sensitivity tests were performed, altering the surface forcing, the internal structure of the flow and introducing clouds. Three simulations were performed in each set of perturbations. The simulations are summarized in Table 1.

The analysis of the simulation in TG indicated that the local terrain at the cape has a significant influence on the flow in the expansion fan region. In the first set of sensitivity simulations, one simulation was thus run without the terrain at the cape (NoTerr) and one run was performed removing the cape entirely (NoCape). Results from TG also indicated that the atmospheric sensitivity to the actual SST field was minor; thus, one sensitivity simulation was here carried out using a more realistic SST field (RealSST), that was estimated from a composite of the radiometric surface temperatures measured by the C-130, flying the pattern shown in Fig. 1b, instead of the constant value from the control simulation (Fig. 2).

In the second set of experiments, attempts were also made to alter the background Fr of the flow.

Table 1. *Summary of the different sensitivity experiments*

Run	Specifics
control	see TG for a detailed account
NoTerr	the terrain at Cape Mendocino is set to 1 m
NoCape	the terrain at Cape Mendocino is removed
WeakInv	inversion strength reduced by 8°C
StrongInv	inversion strength increased by 5°C
WeakWind	geostrophic wind at the surface reduced by 50%
cloud	initial MABL humidity increased by 1.3 g kg^{-1}
cloud+	initial MABL humidity increased by 1.7 g kg^{-1}
cloud++	initial MABL humidity increased by 2.2 g kg^{-1}

In order not to change the dynamic structure of the entire flow, this was first attempted in 2 simulations by changing the initial inversion strength, first decreasing it by 8°C (WeakInv) and then increasing it by 5°C (StrongInv). This should increase and decrease Fr by 38% and 12%, respectively, everything else being equal. Since it was difficult to decrease Fr this way, and still maintain a reasonable inversion, a third simulation was performed with a reduction of the geostrophic v-component at the surface by 50%, to -7.5 ms^{-1} (Weakwind); this decreases Fr by 50%.

Several studies have shown that the presence of clouds at the top of the MABL enhances turbulent mixing and maintains a significantly deeper well-mixed layer (Tjernström and Koracin, 1995; Tjernström and Rogers, 1996). In Tjernström and Koracin (1995) it was also shown that the formation of clouds may act as a bifurcation, i.e., the MABL development when clouds form becomes governed by the cloud field and the future fate of the MABL is totally different from that if clouds do not form. Stratocumulus or stratus are very common along this coast, although, no clouds were present in the observations for 7 June 1996. In the control run, clouds never form. In the 3rd set of sensitivity simulations, clouds are thus artificially introduced at the initial time in 3 simulations, by increasing the initial MABL humidity by 1.3 (cloud), 1.7 (cloud+) and 2.2 (cloud++) g kg^{-1}, respectively. In all these cases, clouds formed during the dynamic initialization, but with different depth and cloud liquid water content. The purpose is to see if the MABL develops differently with clouds present, also in this case.

4. Results

4.1. *The control run*

The control run for 7 June around Cape Mendocino is presented and analyzed in detail in TG. An objective evaluation, by interpolation of model data in 3 dimensions and time along the aircraft track, reveal a good agreement. Flow structure from the model was also compared to the composite analysis of the measurements along several cross-sections and this confirms the evaluation. The control run is thus only discussed briefly here.

Some bulk characteristics of the flow in this

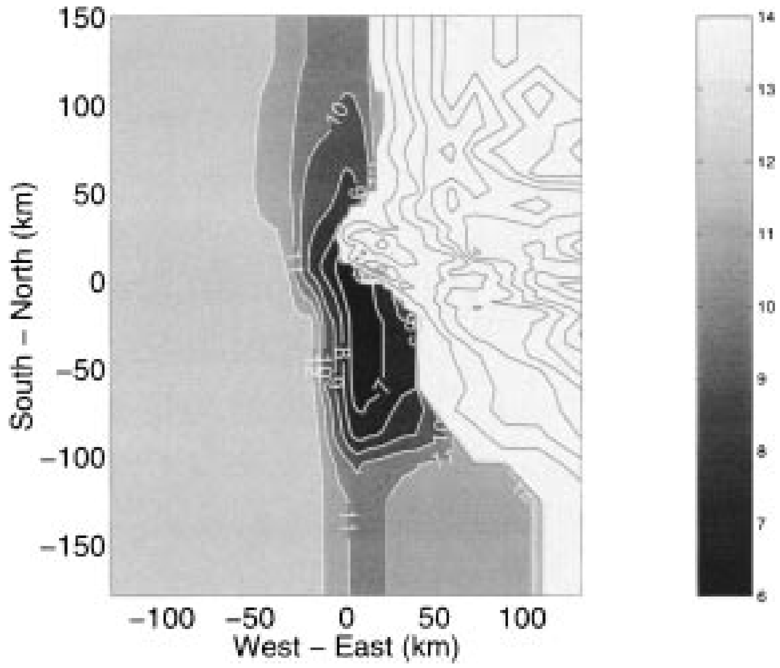

Fig. 2. The SST field (°C) used in the sensitivity simulation with a realistic SST. This was obtained by interpolation from the aircraft measurements on 7 June 1996 (Fig. 1).

case are presented in Fig. 3, showing MABL depth, maximum wind speed and Fr. The MABL depth is here, and elsewhere in this paper, defined as the height when the potential temperature first exceeds the surface value by 1.5°C; this is a simple, although somewhat arbitrary, type of definition also utilized by Dorman et al. (1999). It must be recognized that it only works as long as the MABL is reasonably well mixed. Fr is calculated, combining this depth with the inversion strength, defined as the potential temperature difference taken over a height interval determined by stability, and the mean velocity within the MABL. It could be argued that the wind speed at the inversion height should be used; this would increase Fr by about 20–30%. Fr could also be defined differently, using the maximum the Brunt–Vaissala frequency and the height where this occurs. This ambiguity follows as a consequence of trying to apply the shallow-water theory to a continuously sheared and stratified atmosphere. The exact value of Fr is thus somewhat arbitrary; however, varying these definitions, within reasonable bounds, changes little in terms of the structure shown in Fig. 3c.

In general, the MABL gradually grows deeper with offshore distance (Fig. 3a), reaching above 400 m around $x \sim -180$ km (in model coordinates); this increase continues to the model boundary. Upstream of the cape, there is a slight increase in MABL depth while approaching the coast, due to the blocking of a weak onshore flow, and then it decreases rapidly within 50 km closest to the coast. Downstream of the cape, the expansion fan is clearly seen and the boundary layer collapses from ~ 350 m down to < 10 m in a zone that is widening from ~ 20 km close to the cape, to 200 km at the southern model boundary. There is a gradual increase in the maximum wind speed (Fig. 3b) from ~ 20 ms^{-1} to 23 ms^{-1} close to the coast upstream of the cape, but within the expansion fan, there is a marked increase to an elongated maximum along the largest slope of the inversion, reaching > 28 ms^{-1}. Based on the offshore conditions upstream of the cape, the Rossby radius is here ~ 200 km, and the flow is supercritical, Fr > 1,

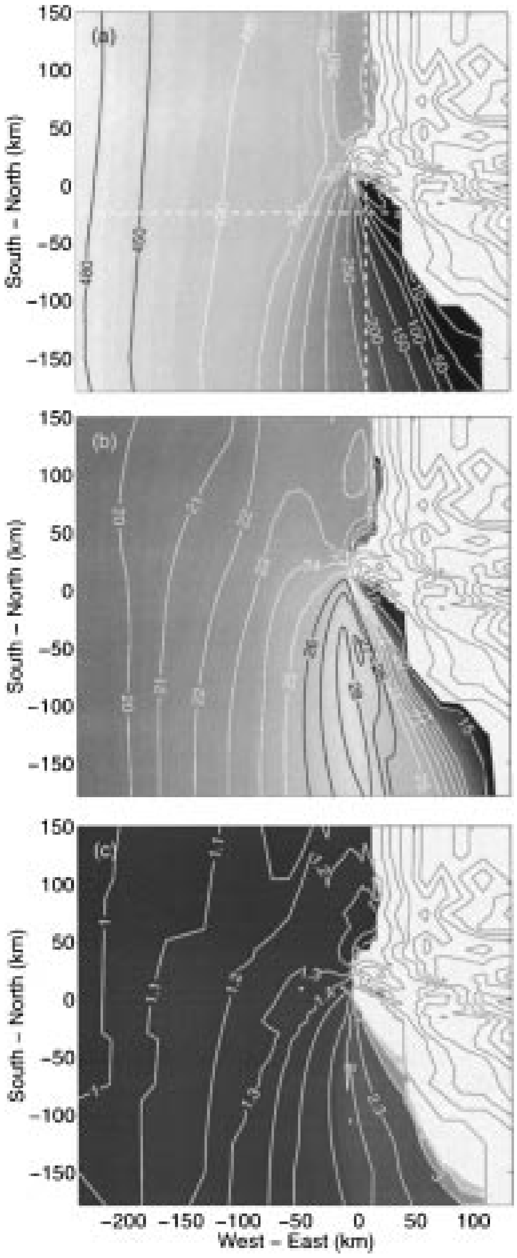

Fig. 3. Contours of some bulk features from the control simulation at 15.00 LT; (a) boundary layer depth (m), (b) maximum boundary layer wind speed (ms^{-1}) and (c) Froude number (see the text for a definition). Also included as a thin dashed line is the positions for the vertical cross-sections used throughout this paper.

within this distance from the upstream coast (Fig. 3c). Further downstream, Fr increases rapidly and in the expansion fan, it reaches $Fr > 4$ in a band along the coast.

Figs. 4a, c show vertical cross-sections of scalar wind speed and potential temperature, along the southern traverse in the flight (Fig. 1b). Similarly, Figs. 4b, d show cross-sections from south to north, across the tip of the cape. In the east–west cross-section, the jet reaching over 28 ms^{-1} is seen, aligned with the maximum slope in the inversion. Immediately above the jet, there is a localized region with very low wind speeds, <4 ms^{-1}; thus, the vertical wind shear is very large; this perturbation reaches well above 2 km. Furthermore, note the total collapse of the MABL between the jet center and the coast (Fig. 4c). These features are also associated with a warming; the temperature at ~ 250 m between the coast and the jet is ~ 10°C higher than the corresponding offshore MABL temperature. Together, these structures cause the jet to have a skewed structure. The north–south cross-section through the cape, hints at a reason for the warming and the low wind speeds inside the expansion fan. Upstream of the cape $Fr \sim 1.2$, while the MABL depth is about the same as the terrain height at the cape. As this terrain is oriented here roughly perpendicular to the flow, it thus causes a partial blocking (Baines, 1995, pp. 38–44). A single lee-wave then forms, that brings down warm air with low momentum from above; note the descending branch of low wind speeds from around $z \sim 2$ km in the upstream air.

4.2. *Changes in surface conditions*

Figs. 5–8 show some results from the sensitivity runs with different surface forcing. The first thing that is obvious from the plots of maximum winds speed (Fig. 5) is that, although there are differences in detail, there is a striking resemblance between all 3 runs. In particular, the run with a more realistic SST (RealSST, Fig. 5c) is very similar to the control run. The main differences are found upstream of the cape, where the offshore winds are here somewhat weaker. At the coast, the wind speed is lower and the along-coast acceleration is somewhat larger; in the control run, the maximum wind speed upstream of the cape is almost constant. However, in the area of the expansion fan, the results are very similar. Similarly, the 2 runs

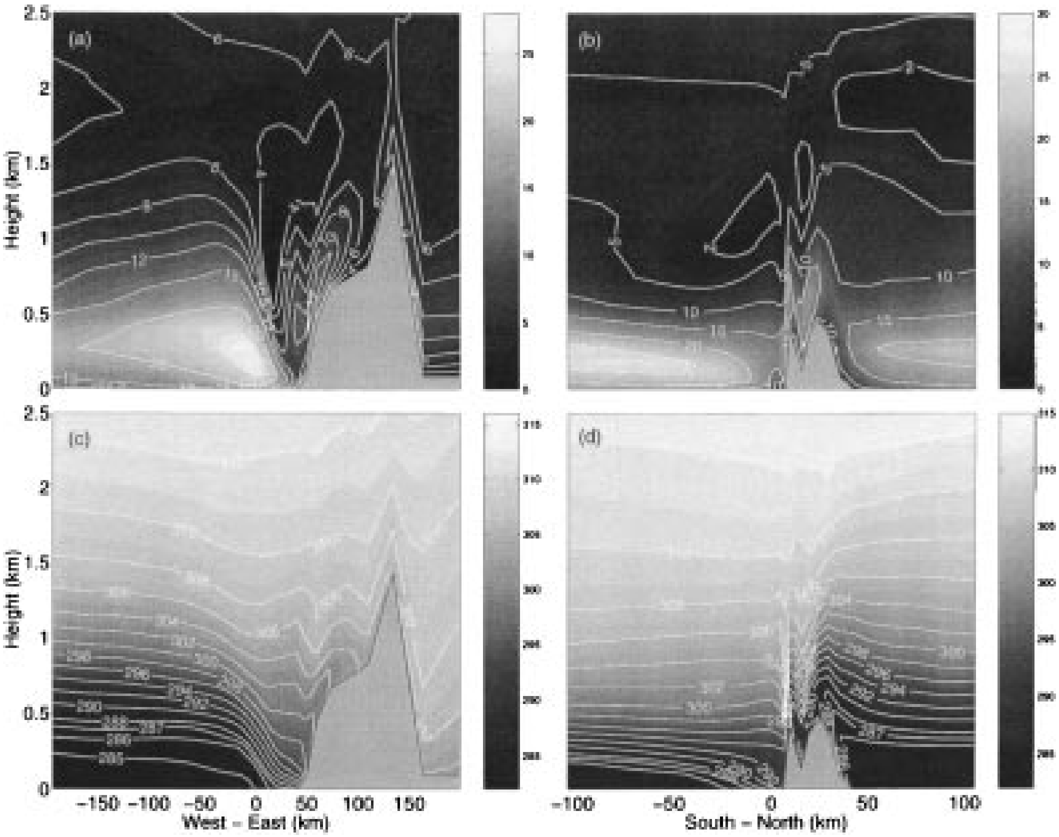

Fig. 4. Vertical cross-sections of ((a) and (b)) scalar wind speed (ms^{-1}) and ((c) and (d)) potential temperature (K) at 15.00 LT from the control run, taken ((a) and (c)) west–east through Shelter Cove and ((b) and (d)) south–north through Cape Mendocino, see Fig. 3.

with altered terrain (NoTerr, Fig. 5a and NoCape, Fig. 5b) are also similar. The locations and elongation of the expansion-fan wind-speed maxima differ slightly, but the magnitude of the maximum wind only differs by $\sim 1\ ms^{-1}$. The run without the cape (Fig. 5b) is the most different, in that the alongcoast acceleration upstream of the cape is more continuous and gradual. Two factors may contribute to this. First, there is a gradual curvature of the coastal terrain, in the absence of the cape, and thus the "channel" is gradually widening. When the cape is present, this gradual curvature is interrupted by the cape. Furthermore, the cape appears to be partially blocking the upstream flow, prohibiting any gradual acceleration here. Second, the terrain is not a homogeneous barrier: the terrain height is very gradually decreasing. This alters the across-flow slope of the terrain which introduces an along-flow baroclinicity in the coastal zone.

In terms of the MABL depth (Fig. 6), there are some differences. Due to the problem of how to analyze the MABL depth in a region where the MABL stratification becomes continuously stable, and the mixed layer disappears, results from RealSST are not shown here. Upstream of the cape, all cases show the slight lifting of the MABL, from the blocking of the weak onshore flow. All the cases feature an expansion fan, although somewhat less predominant in the case without the cape. Following the 300 m isoline, as a proxy for the edge of the expansion fan, it exits the plot at roughly the same location. In terms of the Fr (not shown) all runs, except RealSST, have a similar zone of supercritical flow. In RealSST, this zone is somewhat narrower, as the Fr in this region is

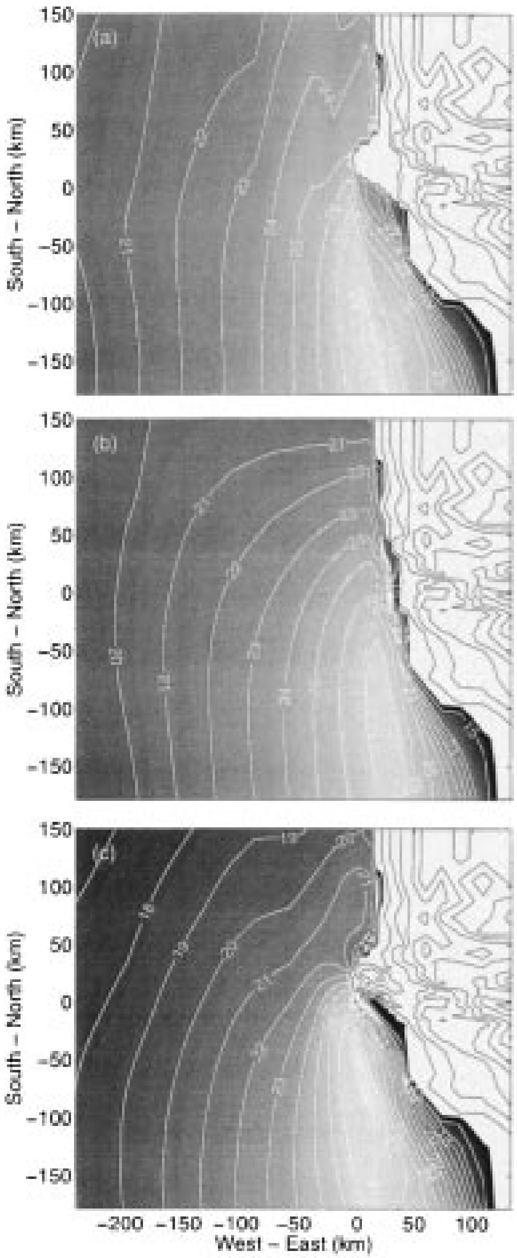

Fig. 5. Contours of MABL maximum wind speed (ms^{-1}) at 15.00 LT for three sensitivity runs: (a) removing the terrain at Cape Mendocino, NoTerr, (b) removing Cape Mendocino, NoCape, and (c) with a realistic SST, RealSST (Fig. 2).

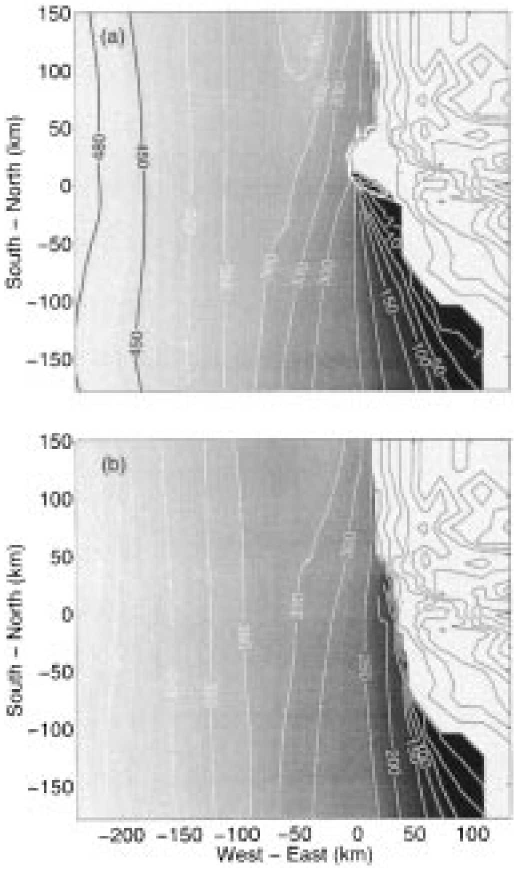

Fig. 6. Contours of MABL depth (m) at 15.00 LT for two sensitivity runs: (a) removing the terrain at Cape Mendocino, NoTerr, (b) removing Cape Mendocino, NoCape.

$\sim$10–20% lower. In general, the run without the cape shows more gradual and smooth transitions, but still with an expansion fan-like behavior.

Fig. 7 shows cross-sections of wind speed and potential temperature from west to east through Shelter Cove (Fig. 3a) for NoCape and RealSST. The cross-sections of wind speed across the expansion fan (Figs. 7a, b) clearly reveal the similarities and differences between the runs. While imposing a realistic SST (Fig. 7b) makes almost no difference at all at this location (Fig. 4a), the runs altering the terrain are clearly different. These two are, on the other hand, virtually identical to each other; only NoCape is shown (Fig. 7a). It is clear that the expansion-fan dynamics governs the flow structure, and altering the SST makes only minor

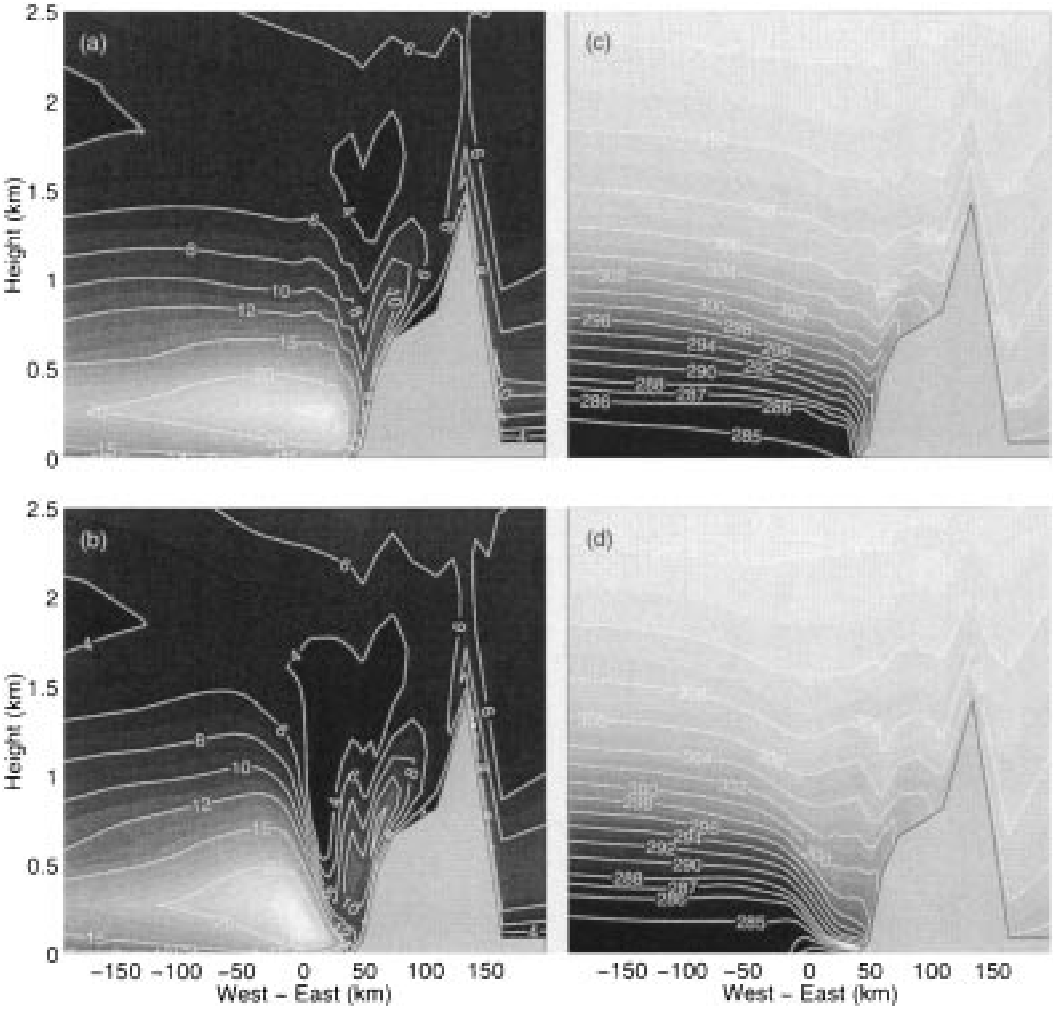

Fig. 7. Contour plots of scalar wind speed (ms^{-1}) at 15.00 LST, in west–east vertical cross-sections through Shelter Cove ((a) and (b)), and south–north cross-sections through the cape ((c) and (d)).The plot shows results for the two sensitivity simulations: ((a) and (c)) without the cape, NoCape, and ((c) and (d)) with realistic SST, RealSST, see Fig. 2.

differences to the wind field. Removing the terrain at the cape alters the jet, removing the skewed shape apparent in the control run (Figs. 4a, 7a), and the area with lower wind speed above the jet, at $z \sim 1$–2 km in the lee of the cape is also almost entirely removed. Removing the cape entirely does not change the flow much more, although the jet axes are moved a short distance further east. Thus, the formation of the expansion fan is a result of where and how the coastline turns. With a cape, but without its terrain, the expansion fan forms at the tip of the cape, but the jet is symmetric in the vertical. Without the cape, the fan moves eastward, but the shape of the jet remains unchanged. Introducing the terrain does not move the expansion fan, but introduces the vertical skewness in the jet. This skewness is related to the collapse of the MABL in the near-cape region, in Shelter Cove, and is caused by the local terrain and not by the expansion-fan dynamics. This is also clear from the cross-section of potential temperature. Fig. 7d shows the low-level impact on the potential temperature of reducing the SST close to the coast. The stability is much larger here; however, this

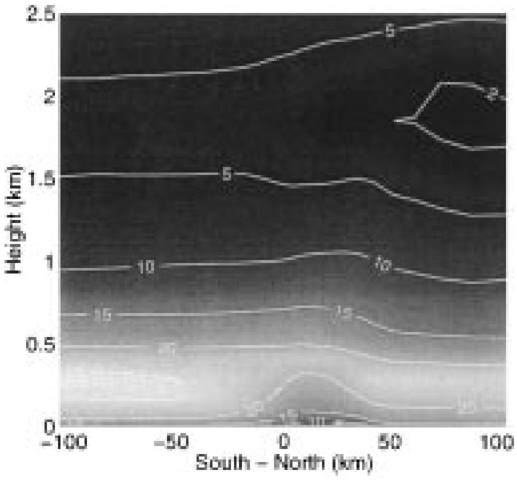

Fig. 8. Contour plot of wind speed (ms^{-1}) in a south–north cross-section through the cape for the case without terrain at the cape, NoTerr.

effect is confined below ~ 100 m, and the wind field is almost not affected at all. In the runs with altered terrain, the perturbation in the temperature field aloft, above Shelter Cove, is much weaker and the structure of the inversion close to the coast is square-shape and much less skewed. The less pronounced lee-wave is also clear from Fig. 8, showing the south–north cross-section of wind speed for the run NoTerr. In the runs with terrain at the cape (Fig. 4b) there is a clear lee-wave at the cape which is absent in both runs without terrain at Cape Mendocino. There are, not surprisingly, differences between NoTerr and NoCape at lower level at the cape, since in the run with the cape but without the terrain, this is a heated land area, while when the cape is removed, this is an ocean surface. However, disregarding the area at and immediately around the cape ($50\text{ km} < y < -50\text{ km}$), the remainder of the low-level wind field is quite similar in all these cases.

In summary, imposing a realistic SST field only resulted in minor effects. The flow must be governed by the expansion-fan dynamics to such a degree that even large changes in the turbulent heat flux, and thus the stability, at the surface have only local and small effects (Burk and Thompson, 1996; TG). Secondly, the skewed shape of the jet, the abrupt collapse of the MABL in Shelter Cove and the local area with warm air and low wind speed above the jet are all caused by the local terrain on the cape, which is almost perpendicular to the flow. This terrain partially blocks the flow upstream of the cape and triggers a single lee-wave (Burk and Thompson, 1996) that propagates up to ~ 3 km. This wave brings down warm and slow-moving flow from aloft, almost all the way to the surface; this feature vanishes almost completely if this terrain is removed. Further removing the cape completely does not change this feature much more. Finally, the expansion fan is also present when the cape is removed, leaving just the gradual curvature of the main coastal mountains. The gradual curvature of the coastal mountains appears sufficient to excite this phenomenon, when the flow is supercritical; the change in coastline orientation does not have to be abrupt. However, with no cape present, the wind speed starts to increase along the upstream coast, even when the flow is supercritical. This may be due to the continuous curvature of the coastline, rather than the abrupt cape, or to effects related to the varying height of the coastal terrain, continuously getting lower further south.

4.3. Changes in internal structure

Similar to the previous section, Figs. 9–13 show the sensitivity runs with different internal structure, to be compared with the control run (Figs. 2, 3). In Figs. 9, 10, showing the Fr and the MABL depth, an unexpected feedback revealed. With a weaker inversion (WeakInv, Fig. 10a), the denominator in the definition of Fr should become smaller, and thus Fr should increase, here by $\sim 40\%$. However, the far offshore Fr is now actually about 10% lower, and this difference gradually decreases into the expansion fan, where the results become very similar to the control run (Fig. 3c). The run with the stronger inversion (StrongInv, Fig. 10b), expected to have a lower Fr by $> 10\%$, reveals a slightly higher Fr, except for far upstream. For this case, the structure is also slightly different. The zone with supercritical flow widens downstream to the cape, while in the control run, this width was almost constant. Also here, the differences disappear in the expansion fan. Only the case where the background flow speed is reduced by 50%, is significantly different (LowWind, Fig. 10c). Here, the flow upstream of the cape is clearly subcritical, due to the lower wind speed. As the flow approaches the cape, the wind speed

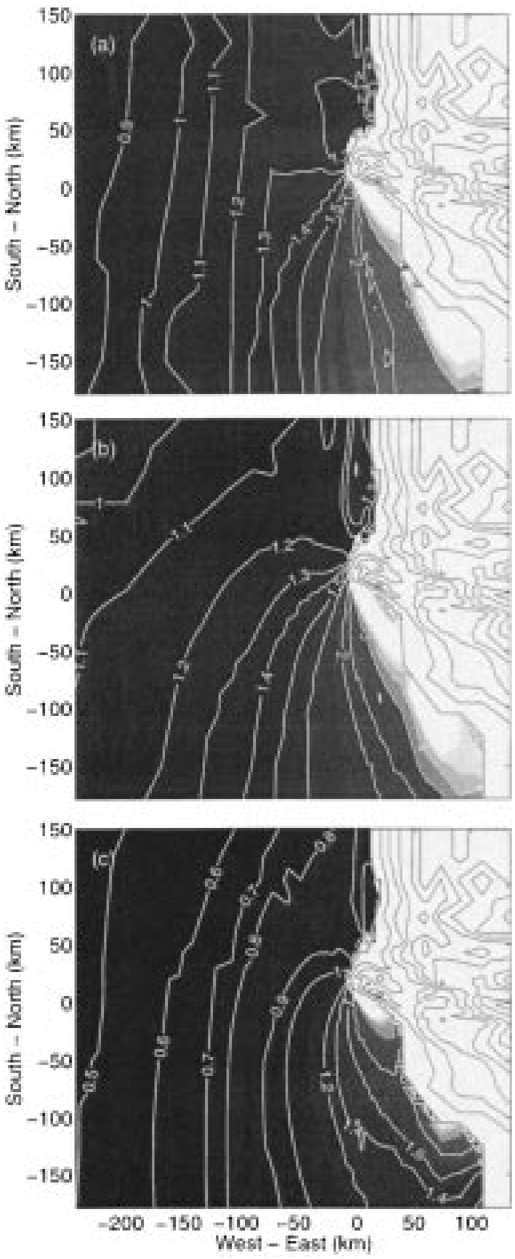

Fig. 9. Contours of the Fr at 15.00 LST for three sensitivity runs: (a) decreasing the inversion strength, WeakInv, (b) increasing the inversion strength, StrongInv, and (c) decreasing the background (geostrophic) wind speed by 50% below 2500 m, WeakWind — see the text for a discussion.

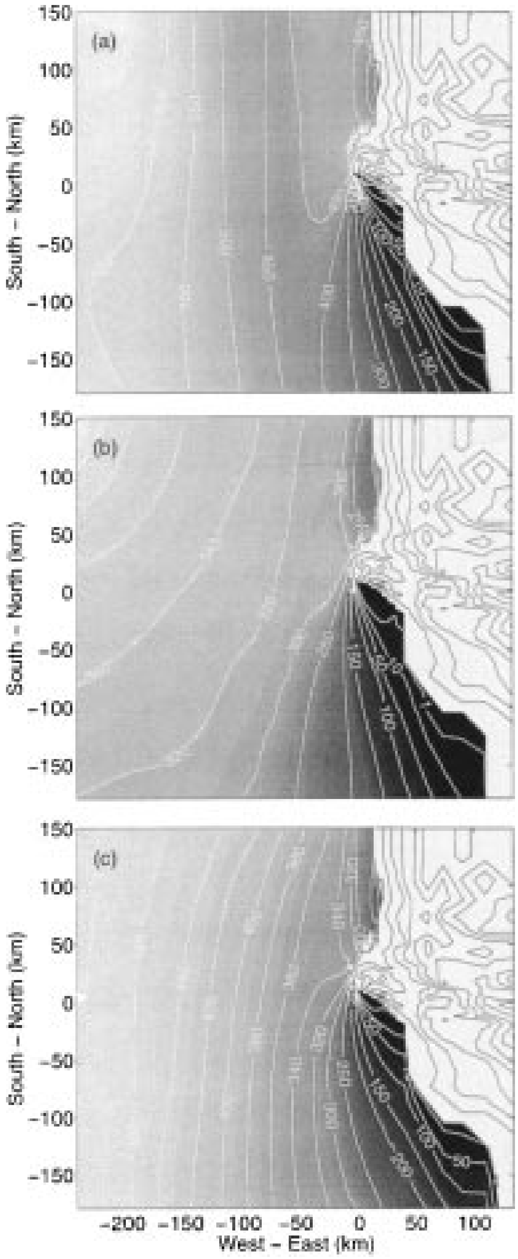

Fig. 10. As Fig. 10, but for MABL depth (m).

increases sufficiently for the Fr to become supercritical; the flow is transcritical.

The contradictory behavior for the cases with the different inversion strength is explained in Fig. 10, showing the MABL depth. Decreasing the

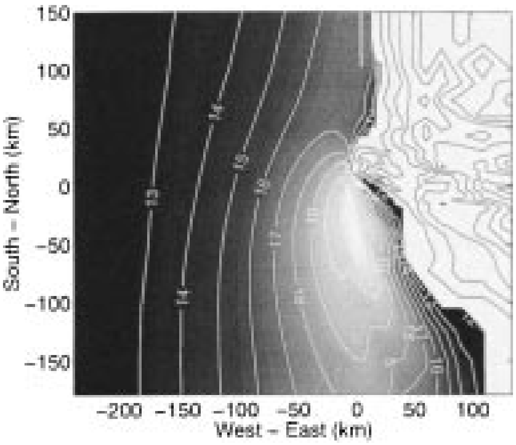

Fig. 11. Contours of MABL maximum wind speed (ms^{-1}) at 15.00 LT for WeakWind, the case with decreased the background (geostrophic) wind speed.

inversion strength by as much as 8°C, enhances the ability for turbulent entrainment at the inversion to mix air from above into the MABL. Consequently the MABL becomes deeper, and this compensates for the weaker inversion strength in the expression for the gravity-wave phase speed. When the inversion is stronger, the opposite occurs, but only to a lesser degree, since the original inversion was already quite strong; strengthening it further has less influence than weakening it. Consequently, the MABL in WeakInv (Fig. 10a) is about 200 m deeper offshore. This difference becomes smaller in the expansion fan, and decreases to 20 m into Shelter Cove. In StrongInv (Fig. 10b), the offshore MABL depth is more variable, from 400 m to the north-west and then decreases by $\sim 0.3\ \mathrm{mkm}^{-1}$, going due south. In the expansion fan, the difference becomes smaller; however, this MABL continues to be shallower than the control run, by from 70 m at the edge of the expansion fan to ~ 10 m at the coastline. These results must be critically dependent on the amount of wind shear in the inversion. Here, with a low-level jet underlying weaker winds aloft, this shear is large. On the other hand, such conditions appear to be common along this coast, and without this jet, the upstream flow would probably not be supercritical in the first place, and thus this mechanism would be less interesting. In these 2 simulations, the changes in the marine boundary layer depth almost completely cancelled

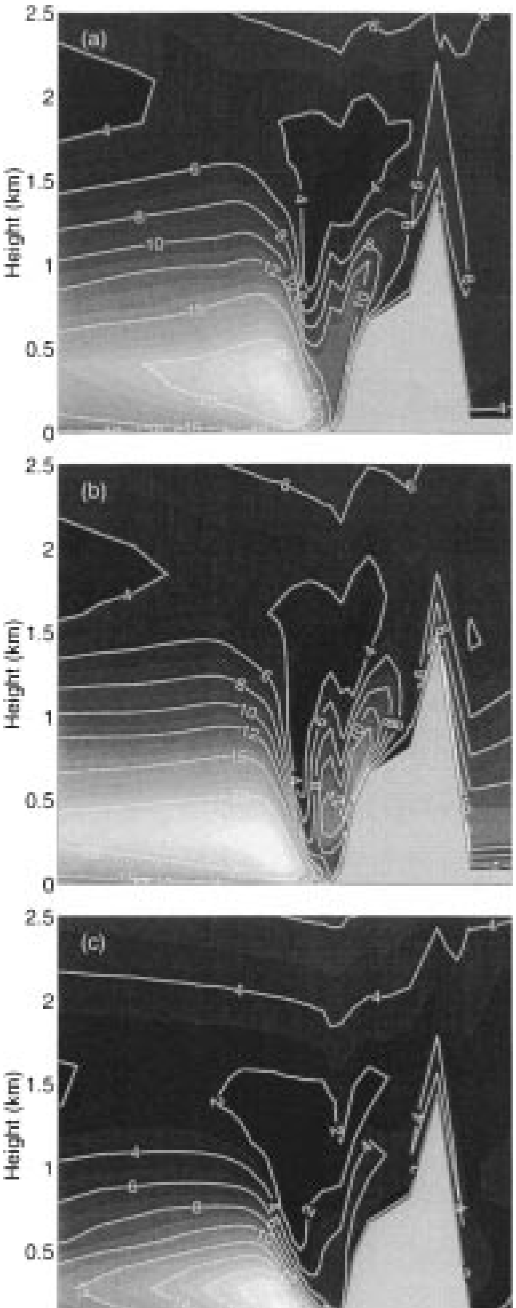

Fig. 12. Contour plots of scalar wind speed (ms^{-1}), in a vertical west–east cross-section through Shelter Cove, for the three sensitivity simulations in Figs. 9, 10.

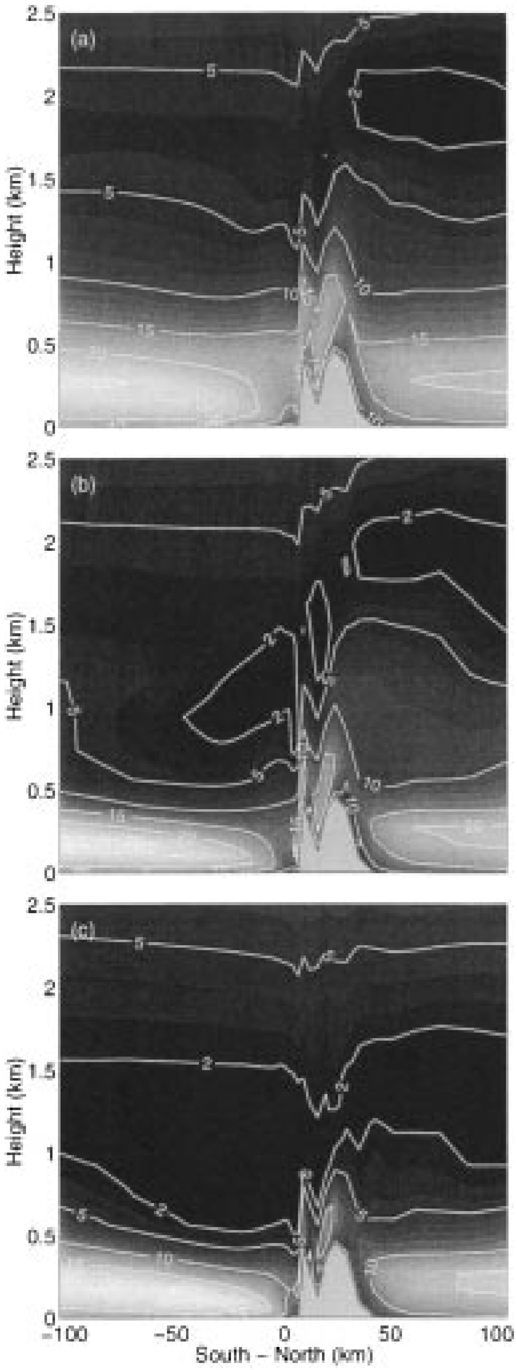

Fig. 13. Contour plots of scalar wind speed (ms^{-1}) at 15.00 LST, in a vertical south–north cross-section through Cape Mendocino, for the 3 sensitivity simulations in Figs. 9, 10.

the changes in Froude number by altering inversion strength. This may be a fortuitous result, in that the details may be specific to this case. It must also be recognized that entrainment in any model is critically dependent on details of the turbulence closure.

The wind speed patterns in these cases are also very similar, although the maximum winds reach somewhat different magnitude. For the deeper MABL, the wind speed is, as expected, somewhat lower, but the difference is only a few ms^{-1}. Similarly, the shallower MABL has maximum winds that are a few ms^{-1} larger; here, the patterns offshore and upstream are also different, with more acceleration along the upstream coast, in particular offshore. Only the case where the background wind speed is reduced by 50% (WeakWind) is shown in Fig. 11. This case also has a similar pattern, but at a significantly lower wind speed. Note however that in relative terms, this transcritcal case is more super-geostrophic than the other cases. The 7.5 ms^{-1} reduction in background flow, translates into a reduction of the maximum wind speed of ~ 8 ms^{-1}, compared to the control run. Thus the absolute magnitude of the super-geostrophic fraction of the wind is about as strong here as for the other cases. Maximum wind speeds are 93, 80, 100, and 193% larger than the geostrophic wind, for the control run and these runs (WeakInv, StrongInv and WeakWind), respectively. The relative increase in wind speed is also the largest for the transcritical run. The increase in wind speed for all 4 cases is similar in absolute terms, about 6–8 ms^{-1}. In terms of the relative increase in maximum wind speed along the coast, this is 32% for the control run, and 28, 36, and 38%, respectively, for the runs where the internal MABL structure is altered.

These features are also illustrated in the west–east (Fig. 12) and south–north cross-sections (Fig. 13) of the wind speed. The cross-shore vertical structure through the expansion fan is very similar in all the runs. The sloping inversion has the same structure, but with different depths, and the jet is skewed in all the cases; an indication that a lee-wave is present in all the cases. The wind speed in these sensitivity runs at this location peaks at 25, 27 and 20 ms^{-1}, respectively, compared to 26 ms^{-1} in the control run. The lee-wave at the cape terrain is significantly weaker for the deeper MABL in WeakInv (Figs. 13a, 4b), as the flow is no longer so effectively blocked, since the MABL is deeper than the terrain height. Consequently, the case with the shallower MABL shows a somewhat stronger lee-wave (Figs. 13b, 4b). One significant difference appears for the case with the lower background wind speed (WeakWind), is that the lee-wave seems to become evanescent (Figs. 12c, 13c). This was also the reason for attempting to change Fr by manipulation of the inversion. The cases with the same background wind speed, and terrain at the cape, all feature a large-amplitude lee-wave. The vertical displacement of the wind speed minimum aloft ranges from $\sim$500 m in WeakInv, with a deeper MABL, to $\sim$1 km when the MABL is shallower (StrongInv). In WeakWind, the wave is significantly weaker and the amplitude has vanished around 1.5–2 km. The amplitude of the perturbation in the isotherms (not shown) below 500 m is actually somewhat larger here than in the control run; however, at 1 km, most of the amplitude of the wave has already vanished; the isentropic surfaces are almost horizontal from 1.5 km and above.

In summary, it turns out to be close to impossible to reduce the Fr to sub-critical values in the lee of Cape Mendocino for the synoptic conditions that prevailed on 7 June 1996. Even simulations with quite drastic changes to the flow speed, still feature a supercritical expansion fan emanating from Cape Mendocino. Manipulation of the Fr by changing the inversion had an opposite effect than expected. This is due to the negative feedback from the turbulent heat flux over the inversion — the entrainment. As the stability in the inversion becomes smaller, the entrainment is enhanced and the MABL grows deeper, and vice versa when this stability is increased. This compensates for the change in temperature difference over the inversion, in the expression for the phase velocity of the shallow-water gravity waves. Changing the background wind speed also changes other dynamic properties in the flow. In this case, the lee-wave triggered by the terrain at Cape Mendocino becomes evanescent. Still, even with the quite moderate geostrophic wind speed of $\sim$8 ms^{-1}, the low-level flow becomes close enough to supercritical, so that the gradual acceleration at the cape causes a transition to supercritical flow. An expansion fan then forms, and the wind speed peaks at values almost three times the geostrophic value.

4.4. *Inclusion of clouds*

The supercriticality of a flow is determined by the flow speed and the depth of the fluid — here the MABL depth. It is well-known that the cloud-capped MABL is generally significantly deeper and more well-mixed than the cloud-free case (Tjernström and Koracin, 1995; Tjernström and Rogers, 1995). This is due to additional buoyancy generated by radiative processes in the cloud. Along the US west coast, stratocumulus or fog are quite common, partly due to the cool surface in response to the upwelling and partly due to the strong inversion that traps moisture evaporated from the ocean surface. Near the coast, fogs are frequent, while off-shore, the cloud layer often lifts to stratocumulus; even further offshore, it breaks up to cumulus, often with a roll structure (Brooks and Rogers, 1997). On 7 June 1996, satellite imagery reveals no or only insignificant cloud cover around Cape Mendocino. In the simulation and detailed analysis in TG, no clouds were found. In this section, clouds were thus artificially introduced at the initial time, in an attempt to study the coupled effect of the clouds on the MABL depth and thus on the supercriticality, and to see if the presence of a cloud field initially alters the MABL development during conditions such as those prevailing here.

Fig. 14 shows the maximum cloud cover for the run with the most moist initial MABL (cloud++), at 03.00 LST and at 09.00 LST, respectively. The cloud cover is obviously decreasing with time. However, there is an increasing cloud cover with increasing initial humidity (not shown). All 3 runs show a clearing in the expansion fan, as the inversion top is lowered below the lifting condensation level, and also show a secondary cloud maximum along the upstream coast, associated with a slightly deeper MABL. Quantitatively, comparing with typical satellite pictures, these patters appear very plausible. However, the clouds are completely gone by noon, and at 15.00 LST, around the time when the research flight was made, the cloud layer has dissipated completely. No reasonable increase in initial MABL humidity could cause the clouds to remain throughout the afternoon. Obviously, subsidence associated with

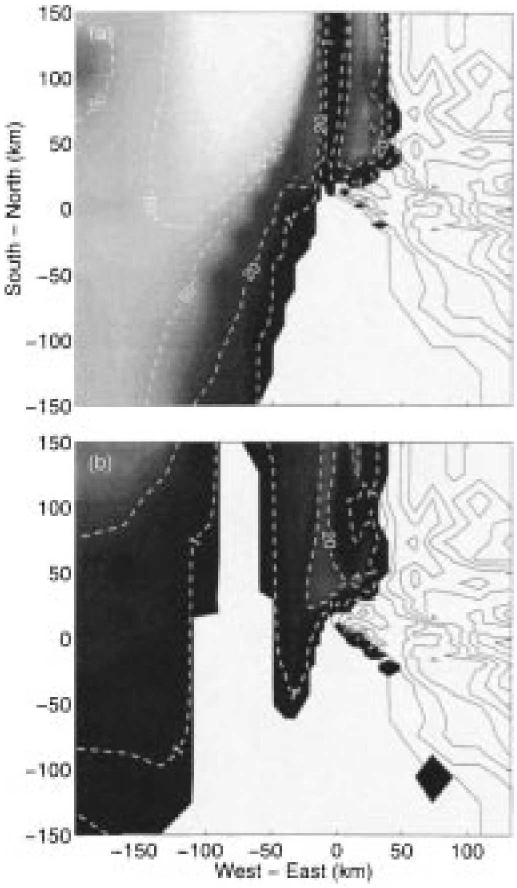

Fig. 14. Contours of cloud cover (%) at (a) 03.00 LST and (b) 09.00 LST from a run with increased initial MABL humidity, cloud++. The cloud cover taken as the maximum cloud fraction in each vertical column in the model.

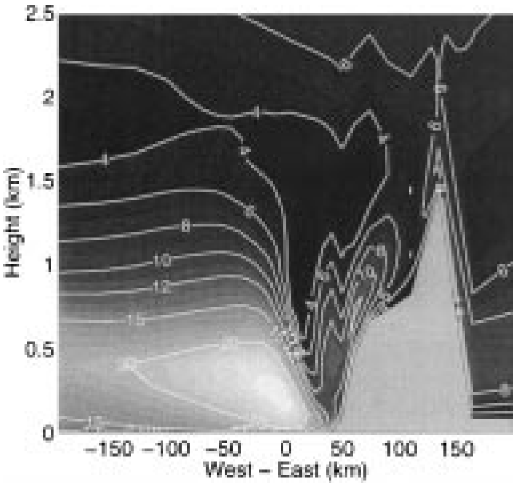

Fig. 15. Contour plots of scalar wind speed (ms^{-1}), in a west–east cross-section through Shelter Cove, for a sensitivity simulation with increased initial MABL humidity.

a secondary circulation along the coast lowers the MABL top along the coast sufficiently to dissipate the cloud layer.

While the clouds last, they do impose changes to the MABL depths, about 200–400 m deeper than in the control run (not shown). When the cloud dissipates, however, the MABL structure quickly reverts to the cloud-free structure in just a few hours. By 15.00 LST, the MABL is still some ~ 150 m deeper than the control run well offshore, while in the expansion fan, this difference disappears completely. Due to different time-history in between the 3 cases, the wind field differs slightly; however, in the expansion fan, the patterns are almost identical to each other and to the control run. Overall maximum wind speeds peak at 27–28 ms^{-1}, and in the west–east vertical cross-section through the expansion fan at Shelter Cove (Fig. 15, only cloud++), the maximum wind speeds are 24–26 ms^{-1}. The jet core seems somewhat more confined to the coast in the cases initialized with clouds. This is expected, since the clouds affected the depth of the offshore MABL the most, thus decreasing the MABL slope offshore and consequently localizing the slope to the near-coast region.

In summary, it was impossible to initialize this MABL so that a cloud cover remained throughout the integration. The clouds were dissipated in the expansion fan, where this is to be expected, due to the strong mesoscale subsidence, but also gradually in the entire model domain. Two things are significant here. First, the presence (or non-presence) of a stratocumulus layer can be governed by both the synoptic scale flow (here imposed by the initial condition and by the background flow) and by the local MABL structure (here governed by the local forcing). It is not obvious, that a cloud layer present at initial time could not intensify the MABL mixing to the extent that the clouds would remain. Such a bifurcation was studied in Tjernström and Koracin (1995). The fact that the clouds dissipate here, indicates that the MABL forcing by the terrain governs the boundary-layer dynamics. Second, the similarity between the flow in the control simulation and the flow where clouds were present up until about noon but then dissipate, indicates the time-scale of the hydraulic control of the flow. In only 3–4 h after the clouds have disappeared, the flow reverts back to almost exactly the same as in the control run, corresponding well with f^{-1}.

The results here indicate that the MABL bulk structure is in this case governed by external forcing, generated by the coastal terrain, and not by MABL dynamics and radiation, as would have been the case in a horizontally homogeneous MABL. Since it is indeed possible to simulate a sustained cloud field on a different day from this experiment, with similar but slightly different synoptic background conditions (for 12 June, unpublished results), the present results warrant a closer examination of the dynamics, of the cloud-capped MABL and its interaction with the coastal dynamics and how this is represented in the model.

5. Discussion and conclusions

The sensitivity of a supercritical coastally trapped marine boundary layer flow to several forcing factors was investigated. Several sensitivity simulations were carried our with a high-resolution mesoscale numerical model. All runs are compared with a control simulation, which is based on a detailed case study presented in Tjernström and Grisogono (1999). This case was observed during the Coastal Waves field experiment on 7 June 1996. The control case has many interesting features; a strong low-level jet along the coast associated with the gradual slope of the MABL inversion causing a supercritical flow, an expansion fan emanating at Cape Mendocino, and lower than expected winds in the lee of the cape. It was also indicated by an analysis of the curl of the wind stress vector, that this flow may be causing the large depression in sea-surface temperature that was observed close to the coast in the lee of the cape. Furthermore, it seemed likely that the local terrain at Cape Mendocino, oriented perpendicular to the flow and having roughly the same height as the marine boundary layer depth, was the cause of the lower wind speed in Shelter Cove. Alltogether, 9 sensitivity runs are examined here; 3 where surface forcing was altered, 3 with different background Froude number and 3 with increased initial boundary layer humidity, causing clouds to form.

Fig. 16 shows a summary of all the 9 sensitivity runs together with the control simulation. For this plot, a location was found along $y = -100$ km in the model domain (Fig. 1) and at the east-west and height coordinate of the highest wind speed within the jet, for each simulation. From this point, back-trajectories were calculated for each run. These were run for 4 h, or until exiting the northern model boundary; Fig. 16a displays all these trajectories. Although there is a spread in the location for the extreme wind speed maximum at the downstream latitude (along $y = -100$ km), many of the trajectories starts up at virtually the same location upstream, with 3 more close by; about 10 km closer to the coast. Only 2 cases are significantly different; the run with the thickest initial cloud, with a history of the deepest MABL (dotted and square), and the run with realistic SST, causing a more sheared flow (dashed and square). In terms of the wind speed along the trajectory (Fig. 16b), the spread in upstream values is a factor of 2, 10–20 ms^{-1}, but in the expansion fan, this spread is reduced to $\sim 10\%$, 25–28 ms^{-1}, except for the case with the reduced background flow. In terms of the relative increase in wind speed along the trajectory (Fig. 16c), the case with the increased inversion strength, and most shallow boundary layer (dashed-dotted with diamond), clearly stands out with an increase to $\sim 2.5\times$ the upstream value. Furthermore, the cases with a lower background wind speed (dashed-dotted with square) and the case without the cape (dashed with diamond) have a large relative wind speed increase along the trajectory, a little less than a factor of ~ 2. The remaining cases are scattered around a 50% increase in wind speed. This can be contrasted with the absolute numbers given earlier. Note here, however, that these values are along a single trajectory. A significant difference here is the difference of the upstream location of the trajectory, which does not necessarily have to be at the upstream wind maximum. Finally, the acceleration along the trajectory is plotted in Fig. 16d. With a few exceptions, the local acceleration at Cape Mendocino turns out to be about the same as for the control run, or slightly larger. Exceptions are the two runs where the local terrain was altered and the most cloudy case, with the

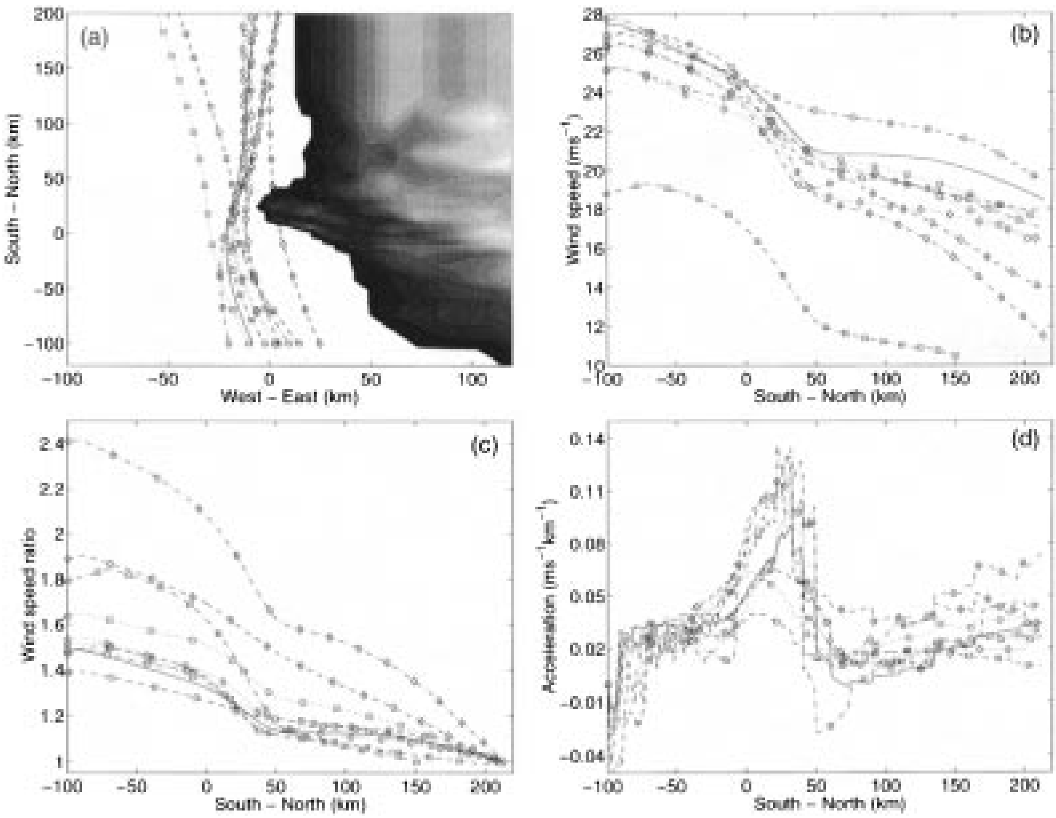

Fig. 16. A summary of horizontal wind speed results from all runs. The values are calculated along back-trajectories from the (x, z)-point at $y = -100$ km where the wind speed is at maximum – see the text for a detailed description. The panels show (a) the trajectories, (b) the wind speed (ms^{-1}) along each trajectory, (c) the wind speed relative to the upstream value for each trajectory and (d) the acceleration along each trajectory. The control run is shown as a solid line. The surface forcing runs are shown as dashed lines (NoTerr — circle, NoCape — diamond, and RealSST — square), the internal structure runs are shown as dashed-dotted lines (WeakInv — circle, StrongInv — diamond, and WeakWind — square) and the cloud runs are shown as dotted lines (Cloud — circle, Cloud+ — diamond, and Cloud++ — square).

deepest boundary layer, that have a less pronounced acceleration. The case with the weaker inversion strength, and consequently a deeper boundary layer also stands out, with more deceleration before the cape but also a quite strong acceleration at the cape. The main impression from these plots is the similarity in the results, in spite of quite drastically varying local forcing. Most trajectories come from about the same upstream location; the largest difference appears to be their initial heights. The difference in upstream height affects the upstream velocity, but since all trajectories (but one) seem to end at about the same wind speed, the relative acceleration becomes different.

The hypotheses from Tjernström and Grisogono (1999) are largely confirmed in this study. The sensitivity run with a realistic sea surface temperature field only produced local differences at low altitude, while the bulk of the flow structure remained the same. Obviously, the dynamical forcing by the supercriticality rules this flow, and more abrupt changes in the surface forcing are required to induce significant changes. Removing the terrain at the cape, or removing the cape entirely, changed the local structure in the region immediately downstream of the cape, removing the area with higher temperatures and lower wind speeds into Shelter Cove, and also removing the skewed shape of the jet. These features are clearly caused by a single lee-wave induced by the flow blocking at the local terrain. It is interesting to note that while removing the cape, only the larger-scale curvature of the coast remains, and still an expansion fan appears. In this case, the acceleration of the flow starts further north and is more gradual. This may be the effect of the curvature of the terrain, which serves as a gradually widening channel, and by the gradually reduced terrain height, that may impose an along-flow baroclinicity. Furthermore, the absence of the cape prevents blocking of this flow.

Attempts to change the Froude number by manipulations of the inversion strength were impeded by an unexpected feedback from turbulent entrainment at the inversion. As the inversion strength was reduced, which should lead to an increase in the Froude number, the entrainment also increased and deepened the boundary layer, which counteracts the expected increase in Froude number, and vice versa when decreasing the inversion strength. More simulations must be carried out to investigate this, before a more general conclusion can be drawn. However, the feedback mechanism seems plausible and although different closures might provide a feedback with a somewhat different gain, the present results are by no means unrealistic. The only way to generate a subcritical flow was to reduce the background flow. Still, even with a 50% reduction, causing subcritical flow upstream of the cape, the flow turns supercritical at the cape. This transcritical case is the one with the most super-geostrophic wind speed, the largest along-coast acceleration of the flow and the largest dynamic non-linearity. However, the weaker upstream flow also alters the lee-wave dynamics at the cape and weakens the downward transport of warm and low-momentum air, as the lee-wave becomes evanescent.

Finally, the attempts to generate clouds in these simulations were unsuccessful. Even with almost unrealistically dense and deep clouds at initial time, the entire cloud field had dissipated by noon on the day in question. This indicates that mesoscale dynamics govern boundary-layer structure in this case. More simulations with and without clouds, for other days during the Coastal Waves 1996 experiment, will help clarify the interaction between the dynamics of the cloud-capped MABL and the mesoscale dynamics along this coast. Interesting to note here, however, is the time it took for the flow to adjust to the coast after the cloud dissipated, and thus relax towards the same features in the control run. This was only ~ 3–5 h. After that time, smaller differences still appear, but the bulk properties of the flow in these simulations are very similar, and the flow in the expansion fan is almost identical to the control run.

In summary, the features of the flow that were observed on 7 July 1996 at Cape Mendocino, and that were subsequently simulated and analyzed in detail by TG, are surprisingly persistent. Even relatively large manipulations of the forcing, the internal flow structure or the thermodynamics, resulted in only minor changes in the final flow structure. This suggests that the type of flow experienced on 7 June during the coastal waves experiment is quite common, thus answering in part one of the underlying questions motivating the Coastal Waves 1996 experiment (Rogers et al., 1998), also addressed by Dorman and Winant (1995). The patterns of the Froude number found in these simulations are thus quite consistent for this location, almost self-similar. This is true even with the removal of the entire cape, leaving just the large-scale curvature of the coastal mountains. This feature is potentially useful for local wind forecasting based on weather prediction models with significantly lower resolution. These results indicate that if the wind and offshore boundary-layer depth for the upstream flow, along a relatively homogeneous coast, can be obtained by a coarse-resolution forecast model, more accurate high-wind warnings can be issued, using this apparent self-similarity in the Froude number.

6. Acknowledgments

This study was sponsored by the Office of Naval Research through Grant N00014-96-1-0002. The author is grateful to David Rogers, Clive Dorman, Branko Grisogono, Gunilla Svensson, Steve Burk and Tracy Haack for help and suggestions.

REFERENCES

Andrén, A. 1990. Evaluation of a turbulence closure scheme suitable for air-pollution applications. *J. Appl. Meteor* **29**, 224–239.

Baines, P. G. 1995. *Topographic effects in stratified flow*. Cambridge University Press, pp. 88–90.

Beardsley, R. C., Dorman, C. E., Friehe, C. A., Rosenfeld, L. K. and Winant, C. D. 1987. Local atmospheric forcing during the coastal ocean dynamics experiment (1) A description of the marine boundary-layer and atmospheric conditions over a northern California upwelling region. *J. Geophys. Res.* **92**, 1467–1488.

Bond, N. A., Mass, C. F. and Overland, J. E. 1996. Coastally trapped wind reversals along the United-States west coast during the warm-season (1) Climatology and temporal evolution. *Mon. Wea. Rev.* **124**, 430–445.

Burk, S. D. and Thompson, W. T. 1996. The summertime low-level jet and marine boundary-layer structure along the california coast. *Mon. Wea. Rev.* **124**, 668–686.

Burk, S. D. and Haack, T. 1998. Modeling unusual coastal wave clouds. Preprint. *8th Conference on Mountain meteorology*, Flagstaff, AZ. Amer. Meteor. Soc.

Brooks, I. M. and Rogers, D. P. 1997. Aircraft observations of boundary layer rolls of the coast of California. *J. Atmos. Sci.* **54**, 1834–1849.

Cui, Z., Tjernström, M. and Grisogono, B. 1998. Idealized simulations of atmospheric coastal flow along the central coast of California. *J. Appl. Meteor.* **37**, 1332–1363.

Dorman, C. E. and Winant, C. D. 1995. Buoy observations of the atmosphere along the west coast of the United-States, 1981–1990. *J. Geophys. Res.* **100**, 16029–16044.

Dorman, C. E. and Rogers, D. P. 1998. The structure of summer high wind speeds around Cape Mendocino, California. Preprints. *2nd Conference on Coastal atmospheric and oceanic prediction and processes*, Phoenix, AZ. Amer. Meteor. Soc., p. 156.

Dorman, C. E., Rogers, D. P., Nuss, W. and Thompson, W. T. 1999a. Adjustment of the summer marine boundary layer around Pt. Sur, California. *Mon. Wea. Rev.*, in press.

Dorman, C. E., Holt, T., Rogers, D. P. and Edwards, K. 1999b. Large-scale structure of the June–July 1996 marine boundary layer along California and Oregon. *Mon. Wea. Rev.*, in press.

Enger, L. 1986. A higher order closure model applied to dispersion in a convective PBL. *Atmos. Environ.* **20**, 879–894.

Enger, L. 1990a. Simulation of dispersion in moderately complex terrain — Part A. The fluid dynamic model. *Atmos. Environ.* **24A**, 2431–2446.

Enger, L. 1990b. Simulation of dispersion in moderately complex terrain — Part B. The higher order closure dispersion model. *Atmos. Environ.* **24A**, 2447–2455.

Enger, L., Koracin, D. and Yang, X. 1993. A numerical study of the boundary layer dynamics in a mountain valley. Part 1. Model validation and sensitivity experiments. *Bound. Layer Meteor.* **66**, 357–394.

Enger, L. and Grisogono, B. 1998. The response of Bora-type flow to sea-surface temperature, *Quart. J. Roy. Meteor. Soc.* **124**, 1227–1244.

Grisogono, B. 1995. Wave drag effects in a mesoscale model with a higher order closure turbulence scheme. *J. Appl. Meteor.* **34**, 941–954.

Grisogono, B. and Tjernström, M. 1996. Thermal mesoscale circulations on the Baltic coast (2) Perturbation of surface parameters. *J. Geophys. Res.* **101**, D14, 18,999–19,012.

Grisogono, B., Ström, L. and Tjernström, M. 1998. Small-scale variability in the coastal atmospheric boundary layer. *Bound-Layer Meteor.* **88**, 23–46.

Mellor, G. L. and Yamada, T. 1982. Development of a closure model of geophysical flows. *Reviews of Geophysics and Space Physics* **20**, 851–875.

Neiburger, M., Johnson, D. S. and Chien, C. W. 1961. Studies of the structure of the atmosphere over the eastern Pacific Ocean in the summer. In: *The inversion over the eastern north Pacific Ocean*, University of California Press, pp. 1–94.

Overland, J. E. 1984. Scale analysis of marine winds in straits and along mountainous coasts. *Mon. Wea. Rev.* **112**, 2532–2536.

Pielke, R. A. 1984. *Mesoscale meteorological modeling*. Academic Press, 599 pp.

Rogers, D., Dorman, C. E., Edwards, K., Brooks, I., Melville, K., Burk, S. D., Thompson, W. T., Holt, T., Ström, L., Tjernström, M., Grisogono, B., Bane, J. M., Nuss, W., Morley, B. and Schanot, A. 1998. Highlights of coastal waves 1996, *Bull. Am. Meteorol. Soc.* **79**, 1307–1326.

Samelson, R. M. 1992. Super-critical marine-layer flow along a smoothly varying coastline. *J. Atmos. Sci.*, **49**, 1571–1584.

Samelson, R. M. and Lentz, S. J. 1994. The horizontal momentum balance in the marine atmospheric boundary layer during CODE-2. *J. Atmos.Sci.* **51**, 3745–3757.

Svensson, G. 1998. Model simulations of the air quality in Athens, Greece, during the MEDCAPHOT-TRACE Campaign. *Atmos. Env.* **52**, 2239–2268.

Svensson, G. and Klemm, O. 1998. Aircraft measurements and model simulations of the air quality in Athens, Greece. *Atmos. Env.* **52**, 2269–2289.

Tjernström, M. 1987a. A study of flow over complex terrain using a three-dimensional model. A preliminary model evaluation focusing on stratus and fog. *Ann. Geophys.* **88**, 469–486.

Tjernström, M. 1987b. *A 3-dimensional meso-γ-scale model for studies of stratiform boundary layer clouds.*

A model description. Department of Meteorology, Uppsala University, Rep. no 85.

Tjernström, M. 1988a. Numerical simulations of stratiform boundary-layer clouds on the meso-γ-scale. Part I. The influence of terrain height differences. *Bound. Layer Meteor*. **44**, 33–72.

Tjernström, M. 1988b. Numerical simulations of stratiform boundary-layer clouds on the meso-γ-scale. Part II. The influence of a step change in surface roughness and surface temperature. *Bound. Layer Meteor*. **44**, 307–230.

Tjernström, M. and Koracin, D. 1995. Modelling the impact of stratocumulus on boundary layer structure. *J. Atmos. Sci*. **52**, 863–878.

Tjernström, M. and Rogers, D. P. 1996. Turbulence Structure in Decoupled Marine Stratocumulus: A case study from the Astex field experiment. *Journal of Atmospheric Sciences*, **53**, 598–619.

Tjernström, M. and Grisogono, B. 1996. Thermal mesoscale circulations on the Baltic coast (1) A numerical case study. *J. Geophys. Res*. **101**, D14, 18,979–18,997.

Tjernström, M. and Grisogono, B. 1999. Simulations of super-critical flow around points and capes in a coastal atmosphere. *J. Atmos. Sci*., in press.

Winant, C. D., Dorman, C. E., Friehe, C. A. and Beardsley, R. C. 1988. The marine layer off northern California — an example of supercritical channel flow. *J. Atmos. Sci*. **45**, 3588–3605.

Zemba, J. and Friehe, C. A. 1987. The marine atmospheric boundary-layer jet in the coastal ocean dynamics experiment. *J. Geophys. Res*. **92**, 1489–1496.